

The Gravitationally-Lensed Radio Source MG 0751+2716

Submitted to AJ: 1997.02.19. Accepted: 1997.04.15.

J. Lehar¹, B.F. Burke², S.R. Conner², E.E. Falco¹, A.B. Fletcher², M. Irwin³, R.G. McMahon⁴,
T.W.B. Muxlow⁵, P.L. Schechter²

ABSTRACT

We report the discovery of a new gravitationally lensed radio source. Radio maps of MG 0751+2716 show four lensed images, which, at higher resolution, are resolved into long arcs of emission. A group of galaxies is present in optical images, including the principal lensing galaxy, with a much brighter galaxy just a few arcseconds away. We have measured the redshift of this brighter galaxy. No optical counterpart to the background source has been detected. Lens models that can readily reproduce the lensed image positions all require a substantial shear component. However, neither the very elongated lens nor the bright nearby galaxy are correctly positioned to explain the shear. Lens models which associate the mass with the light of galaxies in the group can produce an acceptable fit, but only with an extreme mass-to-light ratio in one of the minor group members.

Subject headings: Gravitational Lenses — Dark Matter — Radio Sources: individual (MG 0751+2716)

¹ Center for Astrophysics, 60 Garden St, Cambridge, MA 02138, USA. jlehar@cfa.harvard.edu

² Mass. Inst. of Technology, Dept of Physics, 77 Mass. Ave, Cambridge, MA 02139, USA

³ Royal Greenwich Observatory, Madingley Rd, Cambridge, CB3 0EZ, UK

⁴ Institute of Astronomy, Madingley Rd, Cambridge, CB3 0HA, UK

⁵ Nuffield Radio Astronomy Laboratories, Jodrell Bank, Cheshire SK11 9DL, UK

1. Introduction

The past decade has seen great progress in the study of gravitational lensing (*e.g.*: Schneider *et al.* 1992; Blandford & Narayan 1992). Since extragalactic radio sources are typically at high redshift, radio surveys have proven to be very effective for finding lensed systems. The MG-VLA (Lawrence *et al.* 1986; Hewitt 1986; Lehar 1991; Herold 1996), JVAS (Patnaik *et al.* 1992), and CLASS (Myers *et al.* 1995) radio searches have between them found about half of the ~ 20 confirmed cases, at a rate of approximately one lensed system per thousand sources. Most of these systems have extended structures in the radio which can provide many lens model constraints.

Here, we present the discovery of a sixth lensed system from the MG-VLA search, and later observations which support the lensing interpretation. We also use the radio components to determine lens models, and compare the lensing mass to the observed luminosity distribution of the foreground galaxies.

2. Observations

MG 0751+2716 was discovered as part of the MG-VLA search, and a number of NRAO Very Large Array (VLA) observations were acquired shortly thereafter (see Table 1). The VLA observations were performed in standard continuum mode, interleaved with observations of J0746+25, 3C 286, and OQ 208, to calibrate the antenna phases, flux scales and polarizations, respectively. Calibration and mapping were performed using standard VLA procedures. The maps were further self-calibrated twice, except for the 2 cm map, which had insufficient dynamic range. The resulting maps have rms noise levels of about twice the thermal limit. Figure 1 shows the VLA maps, with the components named in order of decreasing 3.6 cm peak flux density. There are four components, separated by $\approx 0''.8$, with a morphology similar to that of the lensed system MG 0414+0534 (Hewitt *et al.* 1992). Polarized emission was only detected at 3.6 cm, where all four components show the same linearly polarized fraction and orientation. Slight flux density variations are seen between the two 3.6 cm observations ($\sim 5\%$ in the B component), but their significance is marginal (≈ 2 standard deviations). The radio spectra of the four components agree, and no other radio emission was detected nearby at any frequency. The A1 component on the 2.0 cm map is located at $\alpha=07:51:41.49$, $\delta=+27:16:31.6$ (J2000), with an uncertainty of $\sim 0''.2$ (Lawrence *et al.* 1986). The VLA component photometry (for rectangular apertures) is given in Table 2.

We also observed MG 0751+2716 with the MERLIN array, using six antennae (Cambridge, Darnhall, Defford, NRAL Mk II, Knockin, Tabley). The observations were phase-referenced to the compact calibrator 0743+277, with a 10 min cycle time. The strong point source 2134+004 was used to determine the bandpass and non-closing corrections, and the flux calibration was determined using 3C 286. The antenna polarizations were calibrated using 0743+277 and 3C 286. The data were edited, calibrated and mapped using standard MERLIN analysis procedures, with several iterations of self-calibration. The resulting map resolves the VLA components into long arcs,

with the A and C arcs merging. The arcs are unresolved radially, but significant maxima can be used to identify subcomponents (see Figure 2). The MERLIN A1 component is at $\alpha=07:51:41.48$, $\delta=+27:16:31.6$ (J2000), consistent VLA 2.0 cm position to within $\approx 0''.13$. The positions and peak intensities of the subcomponents are given in Table 3, relative to component A1. No polarized emission was detected in our MERLIN data.

We used the Cambridge Automated Plate Measuring (APM) machine catalog to locate optical counterparts on the Palomar Observatory Sky Survey exposures. No direct optical counterpart was found, but a 19th magnitude galaxy, G1, is located $\sim 6''$ West of the radio source, at $\alpha=07:51:41.04$, $\delta=+27:16:32.6$ (J2000). The astrometric uncertainty of the APM catalog is $\sim 0''.5$.

We obtained an optical spectrum of G1, using the ISIS spectrograph on the William Herschel Telescope at La Palma. We also observed a spectral flux calibration star G191–B2B (Massey *et al.* 1988). The data were reduced following standard procedures in the IRAF software package, and the resulting spectrum is shown in Figure 3. We identified several absorption features common to old stellar populations, yielding a redshift of $z = 0.351$ with an uncertainty of ~ 0.001 . The Mg b absorption is resolved into two lines, separated by $\sim 14 \text{ \AA}$, suggesting an upper limit on the stellar velocity dispersion of $\sigma_v \lesssim 250 \text{ km s}^{-1}$.

A number of optical CCD images were also obtained for the MG 0751+2716 field (see Table 1), using the MDM Hiltner telescope, and the Isaac Newton Telescope (INT) at La Palma. The data were reduced using standard procedures in IRAF. The INT image was taken under photometric conditions and calibrated using the SA 92 field of standard stars (Landolt 1992). The MDM R filter image was then calibrated to the INT observation using a star (Star A) near G1. Figure 4 shows the optical field near MG 0751+2716, with some of the galaxies named in order of increasing distance from G1. We used FOCAS (Valdes 1982) to obtain positions and magnitudes for all the objects on the MDM images, using 5 pixel radius apertures, and limiting magnitudes of $R \approx 25$ and $I \approx 23.5$. The $R-I$ colors are scaled to G1, whose absolute color is unknown. Assuming a flat optical νf_ν spectrum, however, G1 would have $R-I \approx 0.47$. The object positions were calibrated to the APM Palomar data, using twelve stellar objects in the field. Table 4 gives the results for the most relevant objects. A complete listing can be obtained from the authors by request. G3 lies $0''.2$ Northeast of the MERLIN A1 component, coincident within the APM positional uncertainty, and is probably the principal lensing galaxy.

We fitted surface brightness profiles to G1 and G3, using the R filter MDM image. Elliptical profiles were convolved in two dimensions with the observed Star A point spread function. A goodness-of-fit χ^2 was determined by summing the squared differences between the convolved model and the observed data for each pixel, normalized to the off-source sky rms. Three models were considered: a DeVaucouleurs $r^{1/4}$ profile, where R_0 and I_0 refer to the effective radius; an exponential profile; and a Hubble profile. In each case we varied the profile shape, the galaxy position and ellipticity, and the sky level. The best fit was found using an ‘‘amoeba’’ search (Press *et al.* 1989). We estimated the parameter uncertainties from the $\Delta\chi^2 < 1$ intervals, by stepping each parameter

away from the best fit, while optimizing the others. The results are shown in Table 5. The G1 models have excess residuals ($\sim 10\%$ of the peak intensity) near the center of the galaxy, and the exponential model is excluded. The profile parameters R_0 and I_0 are very sensitive to problems with the deconvolution, but the models all give similar ellipticities and orientations. For G3, the models could not be distinguished, but all had consistent ellipticities and orientations.

3. Discussion

MG 0751+2716 is almost certainly gravitationally lensed. The radio morphology is very characteristic of gravitational lensing, and extremely unusual for any other interpretation. As expected for lensed images, the four components have matching radio spectra and polarizations, and the 2.0 cm VLA and 6.0 cm MERLIN maps are in good agreement. There is also a good optical candidate G3 for the lens galaxy, consistent with the radio source position. The lens redshift is not yet determined, but its color, and proximity to G1, suggest that G3 is associated with G1, at a redshift of $z=0.351$.

There is no optical counterpart to the background radio source. Although it is not unusual for lensed radio sources to have very faint host galaxies, any evidence of the source would confirm the lensing and reduce the model uncertainties. Since the radio source has a steep spectrum and is extended, it could be close to the core of its host galaxy, or off to the side in a radio lobe. In the former case, the host galaxy should be visible as a faint ring of arcs around the lens. The present observations, however, lack the sensitivity and angular resolution to detect such a ring. It is unlikely that the host galaxy is off to the side, since the deep 20 cm VLA observation shows no clear evidence of a nearby core or another radio lobe within $1'$. When the 20 cm VLA map is super-resolved with a circular $1''$ restoring beam, a ~ 2 mJy component does appear about $2''$ East of the radio source (along the major axis of the natural radio beam), which coincides with an $R \sim 25$ residual in the optical profile fits to G1; but both the radio and optical detections of this object are marginal at best.

We used the MERLIN components (Table 3) to constrain models of the lensing mass distributions. The lensed image subcomponents are labelled to indicate which are likely to have common background source components (see Figure 2). We used the “lensmod” software (Lehár *et al.* 1993), modified to operate in the image plane. For a given lens model and source component, the fitting algorithm traces the observed images to the source plane, and then finds the model image positions which best correspond to the average source component. A χ^2 goodness-of-fit is then computed from the differences between the observed and model image positions. We used the “amoeba” algorithm (Press *et al.* 1989) to find the parameters with the minimum χ^2 .

As a first approximation, three simple mass models were considered: P+ γ , a point mass lens with an external shear; SIP+ γ , a singular isothermal potential with an external shear; and ESIP, an elliptical singular isothermal potential. These models have five parameters: the lens coordinates

x_L, y_L ; the ring size β ; either an external shear γ or an ellipticity ϵ ; and the major axis orientation angle, ϕ_γ or ϕ_ϵ . The parameter ϵ approximates the $(1 - b/a)$ isodensity ellipticity, derived from the isopotential eccentricity ϵ_{BK} (Blandford & Kochanek 1987). The best fit parameters are given in Table 6, with uncertainties derived from the $\Delta\chi^2 < 1$ ranges. None of these simple models provides a satisfactory fit to the observed images. Moreover, the orientations of the best fit lens models are consistent with neither the ellipticity of G3 nor the location of G1 relative to G3.

Because our single-mass models failed, we explored models which approximate the effects of the nearby galaxies: G3+SIP, an ESIP with its orientation constrained to have $\phi_\epsilon = \phi_{G3}$ (see Table 5), and an additional SIP which can be freely adjusted and moved to a position specified by the polar coordinates r_{ext} and ϕ_{ext} (with an effective shear of $\approx \beta_{ext}/r_{ext}$); G3+Grp, an ESIP constrained to ϕ_{G3} , with four external SIPs, at the positions of the other galaxies in the group, and with ring sizes β_{Gi} proportional to the square-root of their optical brightnesses (see Table 4), scaled to β_{G1} (assuming a common redshift of z_{G1} for all the group galaxies); and G3+4G, like G3+Grp, but with independently adjustable group member ring sizes. The G3+SIP model provides a good fit, and the G3+4G does not. The G3+4G model can account for the shear by moving mass to G4. Figure 5 gives a graphic illustration of the fit quality. For all of our models, a common linear arrangement of the source components can reproduce the observed image structures. Assuming $z_{G3} = 0.351$, $H_0 = 75 \text{ km s}^{-1} \text{ Mpc}^{-1}$, $\Omega = 1$, and a flat optical spectral energy distribution (constant νf_ν , or $B-R \approx 1$) with no evolution, the Faber-Jackson relation (as in Fukugita & Turner 1991) implies a velocity dispersion of $\approx 140 \text{ km s}^{-1}$ for G3. This is consistent with an isothermal ring size of $\beta_{G3} = 0''.37 \pm 0''.02$, provided that $z_s \gtrsim 1$. Likewise, G1 has a Faber-Jackson velocity dispersion estimate of $\approx 240 \text{ km s}^{-1}$. This dispersion is consistent with $\beta_{G1} = 0''.8 \pm 0''.1$ for $z_s \gtrsim 0.8$, and with the upper limit from the optical spectrum.

MG 0751+2716 appears to be one of the increasing number of lensed systems which require more shear than can be easily accounted for optically (Keeton *et al.* 1997). The principal shortcoming of the G3+SIP model is that it places the external mass seven standard deviations South of G1. Similarly, the G3+4G model can only account for the image positions if $\beta_{G4} > \beta_{G1}$, despite the fact that G4 is ten times fainter than G1. This peculiar result cannot be easily explained by placing G4 at a different redshift. We computed the expected ring size for a galaxy with an observed magnitude at arbitrary z , assuming a non-evolving flat spectral energy distribution. For a given observed optical magnitude and assumed M/L ratio, a faint lens needs to be more distant, and thus more luminous, to produce a large ring size. We found that for G4 and G3 to have the same M/L ratio, the lens would have to be at $z \gtrsim 30$ with a background radio source at $z > 100$, for any $\Lambda = 0$ cosmology with $\Omega \gtrsim 0.2$. Since G4 cannot reasonably account for the required shear, either there must be a dark concentration of matter somewhere to the South of G1, or G3 must be embedded in a dark halo whose orientation is misaligned with G3 by $> 30^\circ$.

Considerable work remains to be done on this system. The distance to the lens G3 is not known, and the mass estimates depend sensitively on the lens redshift. Nor are the distances known to most of the other galaxies in the group. The source redshift is also unknown, of course, and although the

model results are not very sensitive to z_s , any optical evidence of the background source would be an important confirmation. HST observations are planned that may be able to distinguish the two possibilities for the background source location. We also plan to continue conducting spectroscopic observations of this system to determine redshifts and velocity dispersions for G3 and the other group members. All of our models predict time delays of a few hours between lensed images. Since the radio source is extended, has a steep spectrum, and has not varied strongly over a two-year period it is unlikely that delays can be measured for MG 0751+2716. However, the radio spectrum does flatten towards the West end of the B component, thus offering some hope that there is a compact, variable core. We have obtained deep 2 cm VLA observations which should help determine whether such a core is present, and provide more detail on the lensed images. MG 0751+2716 is well suited for the “lensclean” algorithm (Kochanek & Narayan 1993), in which a model of the background source is constructed to be consistent with the observed extended structures. With C. Kochanek, we have started this analysis, and we hope to obtain more sensitive constraints on the lensing mass distribution.

It is a pleasure to thank Chris Kochanek and Chuck Keeton for help with the lens models, and Karl Glazebrook for help with the optical spectrum. The NRAO is operated by Associated Universities, Inc., under cooperative agreement with the National Science Foundation. Observations reported here were obtained, in part, at the MDM Observatory; a consortium of the University of Michigan, Dartmouth College and the Massachusetts Institute of Technology. IRAF is distributed by the National Optical Astronomy Observatories, which are operated by the Association of Universities for Research in Astronomy, Inc., under cooperative agreement with the National Science Foundation. JL gratefully acknowledges support from NSF grant AST93-03527.

REFERENCES

- Blandford, R., Kochanek, C. 1987, *ApJ*, 321, 658
- Blandford, R.D., Narayan, R. 1992, *ARA&A*, 30, 311
- Fukugita, M., Turner, E.L 1991, *MNRAS*, 253, 99
- Herold, L. 1996, MIT Ph.D. Thesis
- Hewitt, J.N. 1986, MIT Ph.D. Thesis
- Hewitt, J.N., Turner, E.L., Lawrence, C.R., Schneider, D.P., Brody, J.P. 1992, *AJ*, 104, 968
- Keeton, C.R., Kochanek, C.S., Seljak, U. 1997, *ApJ*, to appear, LANL astro-ph/9610163
- Kochanek, C.S., Narayan, R. 1993, *ApJ*, 401, 461
- Landolt, A.U. 1992, *AJ*, 104, 340

- Lawrence, C.R., Bennett, C.L., Hewitt, J.N., Langston, G.I., Klotz, S.E., Burke, B.F., Turner, K.C. 1986, *ApJS*, 61, 105
- Lehár, J. 1991, MIT Ph.D. Thesis
- Lehár, J., Langston, G.I., Silber, A., Lawrence, C.R., Burke, B.F. 1993, *AJ*, 105, 847
- Massey, P., Strobel, K., Barnes, J.B., Anderson, E. 1988, *ApJ*, 328, 315
- Myers, S.T., Fassnacht, C.D., Djorgovski, S.G., Blandford, R.D., Matthews, K., Neugebauer, G., Pearson, T.J., Readhead, A.C.S., Smith, J.D., Thompson, D.J., Womble, D.S., Browne, I.W.A., Wilkinson, P.N., Nair, S., Jackson, N., Snellen, I.A.G., Miley, G.K., de Bruyn, A.G., Schilizzi, R.T. 1995, *ApJ*, 447, L5.
- Patnaik, A.R., Browne, I.W.A., Wilkinson, P.N., Wrobel, J.M. 1992, *MNRAS*, 254, 655
- Press, W.H., Flannery, B.P., Teukolsky, S.A., Vetterling, W.T. 1989, *Numerical Recipes*, (Cambridge: Cambridge University Press)
- Schneider, P., Ehlers, J., Falco, E.E. 1992, “Gravitational Lenses”, (Springer:Berlin)
- Valdes, F., 1982 “Faint Object Classification and Analysis System”, NOAO document (<ftp://iraf.noao.edu/iraf/docs/focas/focas.ps.Z>).

Table 1. Observation Log

Date	Telescope	Wavelength	Exposure	Resol (fwhm)	Noise (rms)
Radio Observations					
1990.05.03	VLA (A)	3.6 cm	2.5 min	0".2	0.29 mJy beam ⁻¹
1992.11.18	VLA (A)	2.0 cm	5 min	0".11	0.53 mJy beam ⁻¹
		3.6 cm	2.5 min	0".20	0.18 mJy beam ⁻¹
		6.2 cm	1.5 min	0".33	0.28 mJy beam ⁻¹
1993.02.03	VLA (BnA)	20.4 cm	15 min	4".2 × 1".4	0.14 mJy beam ⁻¹
1992.11.25	MERLIN	6.0 cm	15.5 hr	0".05	0.089 mJy beam ⁻¹
Optical Spectroscopy					
1992.04.03	WHT 4 m	6992±1800 Å	60 min	2.5 Å/pixel	~5 μJy/pixel
Optical Imaging					
1993.11.19	MDM 2.4 m	<i>I</i> filter	10 min	0".8	~ 24.6 mag arcsec ⁻²
1994.01.10	INT 2 m	<i>R</i> filter	15 min	1".5	25.6 mag arcsec ⁻²
1995.12.18	MDM 2.4 m	<i>R</i> filter	1.8 hr	0".8	26.2 mag arcsec ⁻²

Table 2. VLA Photometry

Component	Wavelength	S_{aper} (mJy)	S_{pol}^a (%)	ϕ_{pol}^a
A+C	2.0 cm	31.11 ± 2.05	0.0 ± 6.6	...
	3.6 cm ^b	61.36 ± 0.90	7.7 ± 1.2	0
	3.6 cm	62.24 ± 0.49	7.6 ± 0.8	+3
	6.2 cm	118.69 ± 0.61	0.0 ± 0.5	...
B	2.0 cm	14.28 ± 1.25	0.0 ± 8.8	...
	3.6 cm ^b	23.48 ± 0.65	12.0 ± 2.1	+4
	3.6 cm	24.75 ± 0.32	9.0 ± 1.3	+7
	6.2 cm	44.09 ± 0.42	0.0 ± 1.0	...
D	2.0 cm	5.73 ± 0.91	0.0 ± 16.0	...
	3.6 cm ^b	11.45 ± 0.49	15.5 ± 4.4	-6
	3.6 cm	12.18 ± 0.30	9.4 ± 2.6	+3
	6.2 cm	17.53 ± 0.36	0.0 ± 2.0	...
TOTAL	2.0 cm	47.75 ± 4.22	0.0 ± 8.8	...
	3.6 cm ^b	103.71 ± 1.52	13.7 ± 1.3	...
	3.6 cm	104.60 ± 0.88	11.7 ± 1.2	...
	6.2 cm	191.16 ± 1.02	0.0 ± 0.5	...
	20.4 cm	412.99 ± 0.42

^a Linear polarization fractional intensity and orientation in degrees from North through East.^b From the 1991.03.05 MG-VLA observation.

Table 3. MERLIN Components

Component	$\Delta\alpha^a$	$\Delta\delta^a$	S_{peak}^b	Source ID ^c
A1	0.000	0.000	24.603	1
A2(?)	-0.037	+0.045	9.265	2 (unused, for ref only)
A3	-0.060	+0.127	4.652	3
A4	-0.067	+0.180	5.086	4
B1	+0.495	-0.270	8.470	1
B2	+0.405	-0.285	7.888	2
B3–B4(?)	+0.315	-0.292	6.127	3,4 (uncertain)
B5	+0.278	-0.292	9.266	5
B6	+0.067	-0.308	0.889	6
C1	+0.082	+0.510	8.971	1
C2	+0.022	+0.450	9.021	2
C3	-0.052	+0.300	5.414	3
C4	-0.060	+0.255	5.020	4
D1–D5	+0.637 ^d	+0.345 ^d	15.315	1,2,3,4,5

^a Offsets are in arcsec from A1, with 8 mas (1 pixel) assumed uncertainties.

^b Peak flux densities in mJy beam^{-1} , not used for model fits.

^c Source identifications (see Figure 2); multiple numbers imply blended components.

^d Assumed a 16×8 mas error ellipse, oriented at $+45$ deg from North through East.

Table 4. Optical Components

Object	$\Delta\alpha^a$	$\Delta\delta^a$	R_{is}^b	R_{ap}^c	$R-I^c$
G1	0.00	0.00	19.09	19.98	0.00
G2	+4.07	-3.59	23.25	22.90	...
G3	+5.83	-0.91	21.31	21.36	-0.04
G4	-0.91	-6.81	22.23	22.24	-0.38
G5	+10.29	-3.64	22.30	22.27	...
Star A	+10.40	+14.78	19.00	19.09	0.11

^a Offsets from G1 are in arcsec.

^b Magnitudes for light enclosed by the $R = 25$ mag arcsec⁻² isophote.

^c Aperture magnitudes within a $1''4$ radius.

Table 5. Optical Profile Models

Model	G1			G3		
	DeVauc	Expon	Hubble	DeVauc	Expon	Hubble
NDOF	7088	7088	7088	229	229	229
χ^2/DOF	2.30	3.64	1.86	1.13	1.17	1.37
$\Delta\alpha$	-0.114 ± 0.006	-0.109	-0.110	$+0.011 \pm 0.003$	+0.011	+0.007
$\Delta\delta$	$+0.107 \pm 0.004$	+0.095	+0.098	$+0.024 \pm 0.003$	+0.030	+0.024
ϵ	0.417 ± 0.003	0.321	0.398	0.49 ± 0.03	0.48	0.45
ϕ_ϵ	$+1.5 \pm 0.4$	-5.0	+1.4	$+16.7 \pm 2.0$	+14.9	+15.9
R_0	1.98 ± 0.02	0.78	0.48	0.27 ± 0.03	0.29	0.0097
I_0	22.77 ± 0.02	20.12	19.75	20.32 ± 0.37	19.70	13.23

Profile center offsets are in arcsec from center of the brightest pixel. Profile ellipticity $\epsilon = 1-b/a$, and major axis orientation ϕ_ϵ is in degrees from North through East. R_0 is the scale radius in arcsec, and I_0 is the surface brightness scale expressed in R mag arcsec⁻². Uncertainties, from the $\Delta\chi^2 < 1$ ranges, are given for the DeVaucouleurs model; those for other models are comparable.

Table 6. Lens Model Results

Model	P+ γ	SIP+ γ	ESIP	G3+SIP	G3+Grp	G3+4G
NDOF	15	15	15	13	15	12
χ^2/DOF	1.78	1.96	3.95	1.10	3.64	1.14
$\Delta\alpha$	+0.346	+0.348	+0.356	+0.344 \pm 0.005	+0.336 \pm 0.004	+0.345 \pm 0.005
$\Delta\delta$	+0.164	+0.164	+0.176	+0.160 \pm 0.005	+0.158 \pm 0.004	+0.163 \pm 0.004
β	0.398	0.402	0.408	0.371 \pm 0.004	0.351 \pm 0.005	0.352 \pm 0.005
γ or ϵ	0.188	0.093	0.344	0.092 \pm 0.024	0.224 \pm 0.018	0.125 \pm 0.026
ϕ_γ or ϕ_ϵ	-116.6	-116.5	-116.2	-163.6 \pm 3.3	-155.5 \pm 2.6	-164.0 \pm 3.3
β_{ext}	0.63 ^{+0.5} _{-0.2}
r_{ext}	4.0 ^{+2.5} _{-1.0}
ϕ_{ext}	-106.9 \pm 2.7
β_{G1}	0.94 \pm 0.06	0.76 \pm 0.08
β_{G2}	(0.060)	< 0.04
β_{G4}	(0.222)	1.11 \pm 0.13
β_{G5}	(0.215)	< 0.04

Lens model center offsets are in arcsec from A1, and ring sizes β , are in arcsec. Orientation angles are in degrees from North through East. External shears stretch images perpendicular to ϕ_γ , which aligns with the tidal mass concentration. For the G3+Grp model, the numbers in parentheses show the other ring sizes, which are directly scaled to β_{G1} . Uncertainties are from the $\Delta\chi^2 < 1$ ranges.

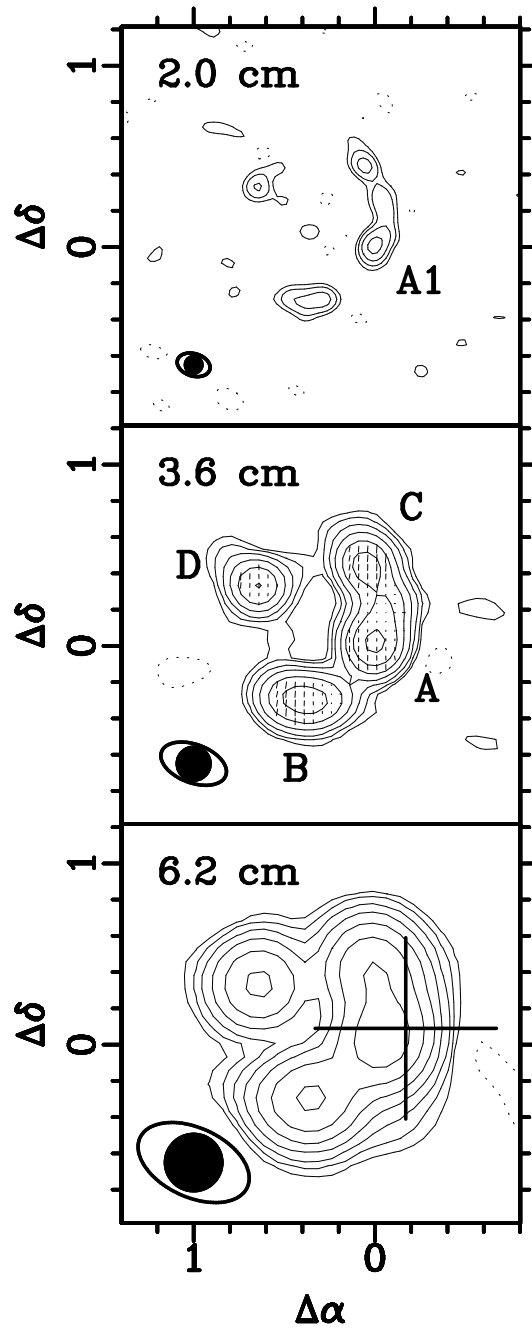


Fig. 1.— VLA maps of MG0751+2716. Offsets are in arcseconds relative to A1. The contours increase by factors of two from $2\sigma_{rms}$, where σ_{rms} is the off-source rms. Fractional polarization vectors are scaled so that one vector spacing corresponds to 20%, and are oriented along the electric field. Each panel shows the fwhm uniform-weighted (open) and restoring (filled) beams. The optical position of G3 is shown as a cross in the 6.2 cm map, scaled to the $\pm 0''.5$ APM astrometric uncertainty.

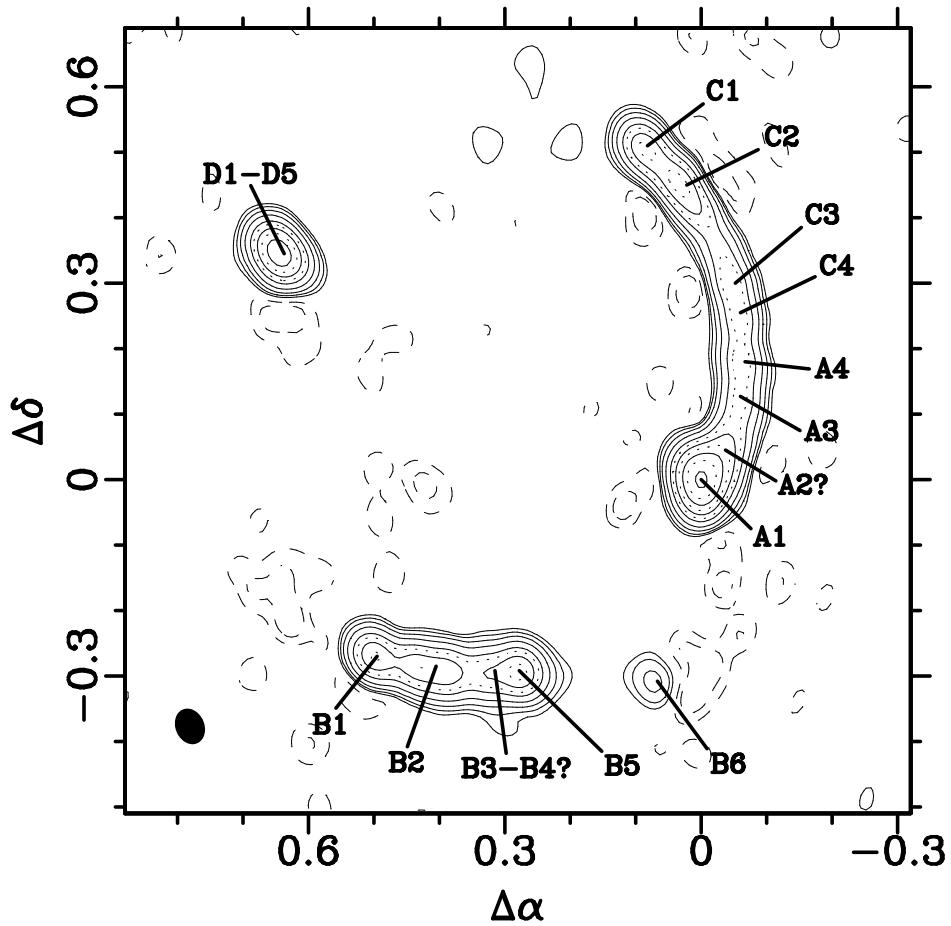


Fig. 2.— MERLIN map of MG0751+2716. Offsets are in arcseconds relative to A1. The contours increase by factors of two from $2\sigma_{rms}$, where σ_{rms} is the off-source rms. Additional dotted contours increase by factors of $\sqrt{2}$ from $32\sigma_{rms}$ to emphasize the labelled subcomponents. The natural-weighted fwhm beam is shown at lower left.

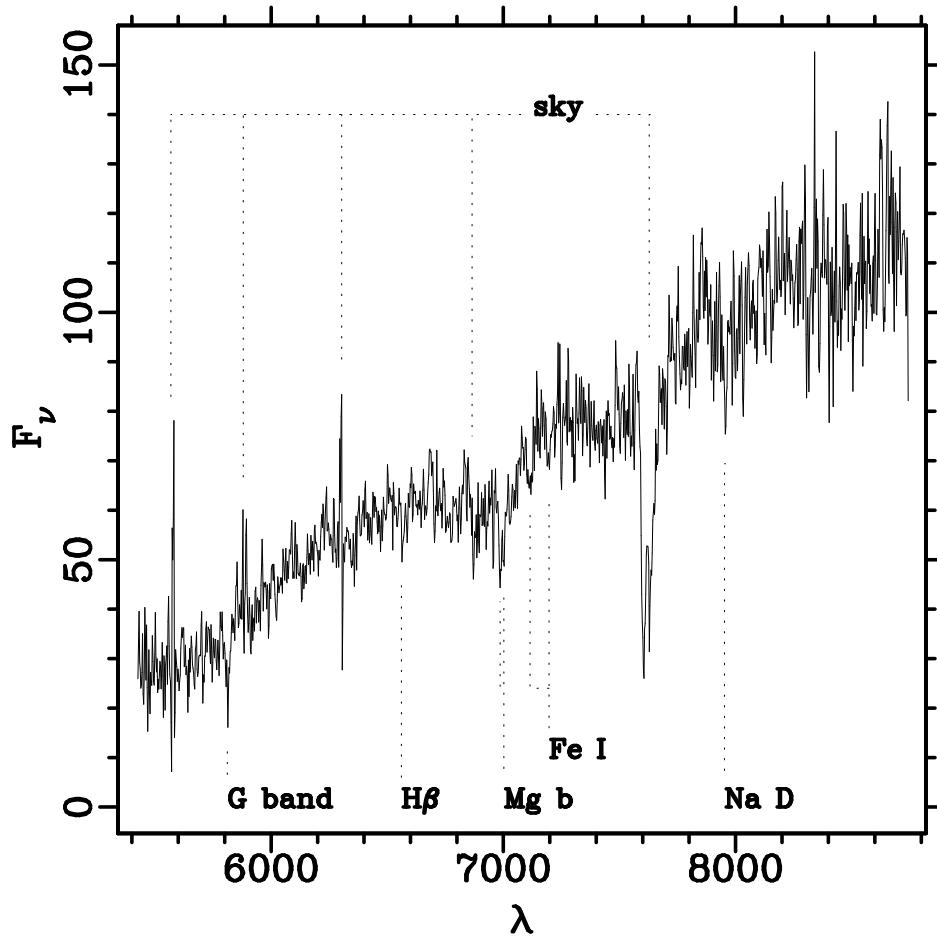


Fig. 3.— Optical spectrum of G1. Wavelength λ is in angstroms, and the flux density f_ν is in μJy . Several absorption features are seen at $z = 0.351$, and some prominent sky features are also labelled.

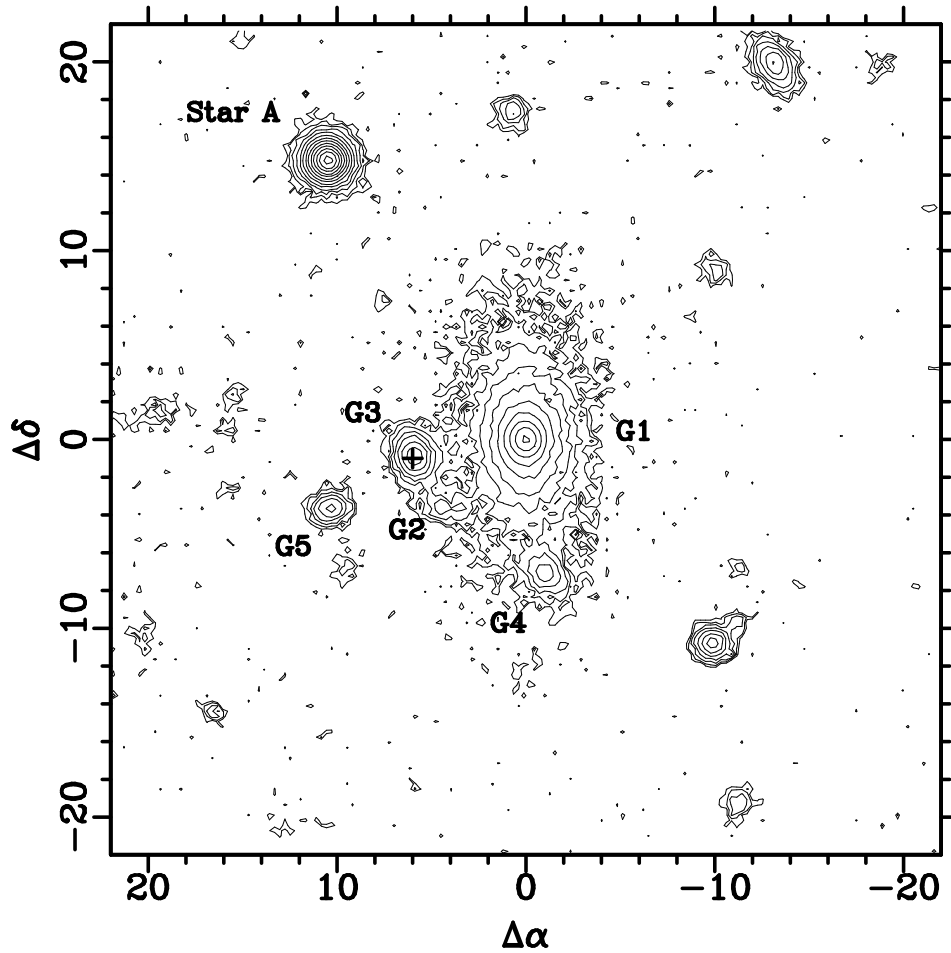


Fig. 4.— Optical field around MG0751+2716, from the MDM R filter image. The contours increase from $2\sigma_{rms}$ by factors of half a magnitude, where σ_{rms} is the off-source rms. Offsets are in arcsec from G1, and the position of the VLA 2 cm component A1 is shown as a $\pm 0''.5$ cross, reflecting the APM astrometric error.

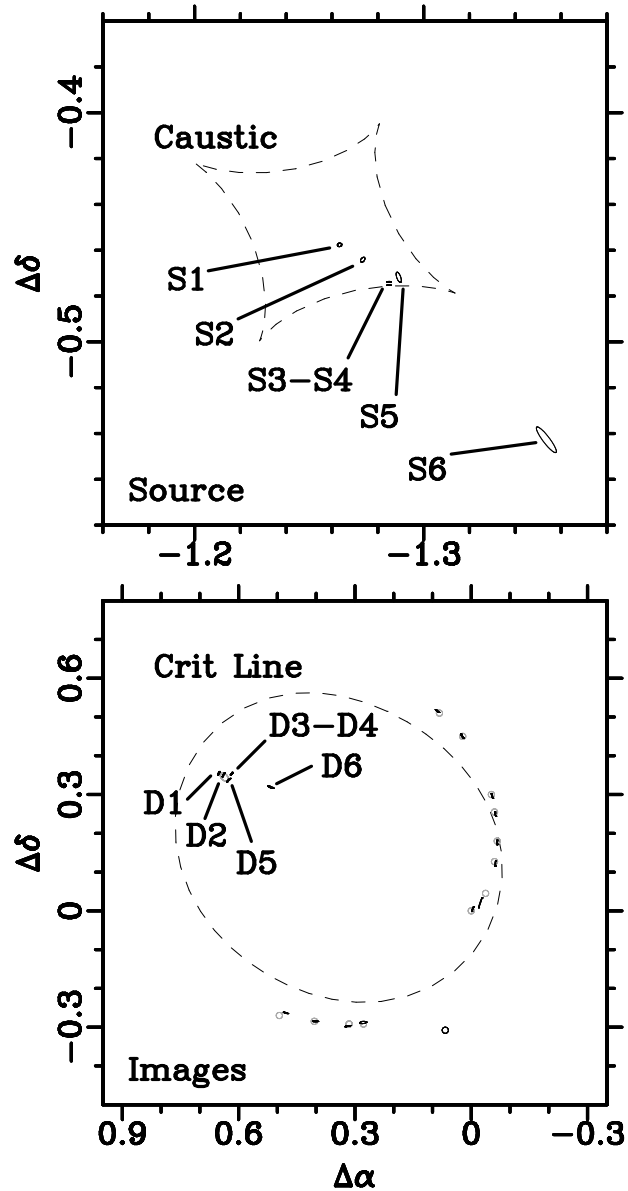


Fig. 5.— Schematic view of the G3+4G lens model. Offsets are given in arcsec from the MERLIN A1 component. The source plane shows the error ellipses for the average source components. The image plane shows these average components projected to the image plane (solid error ellipses), as well as the observed image component positions (dotted error ellipses). The source and D image components have been labelled for reference. Note that the source components are shifted substantially, due to the influence of the group galaxies.